

# Accretion induced black hole spin up in magnetized collapsars

Agnieszka Janiuk<sup>1,a</sup> and Dominika Ł. Król<sup>2</sup>

<sup>1</sup>Center for Theoretical Physics, Polish Academy of Sciences, Al. Lotnikow 32/46,  
P-02-668 Warsaw, Poland

<sup>2</sup>Jagiellonian University Astronomical Observatory, ul. Orła 171,  
P-30-244 Krakow, Poland

<sup>a</sup>[agnes@cft.edu.pl](mailto:agnes@cft.edu.pl)

## ABSTRACT

Black holes are the final stage of gravitational collapse process, and due to the cosmic censorship conjecture, they are created inevitably if a trapped surface has formed in the space-time. The solutions of Schwarzschild and Kerr are describing the spacetime metric for the gravitational field of a spherically symmetric, or rotating black hole. Astrophysically, the rotating black holes of stellar mass are end products of stellar evolution, when the progenitor star was massive enough and possessed a substantial amount of angular momentum. They can be discovered when leaving behind a luminous transient in a form of gamma ray burst, which is followed by an afterglow emission at lower energies and associated with the emerging supernova-like spectra that trace the chemical composition of expanding shells from the explosion. The gravitational binding energy of the massive progenitor star is released in the supernova explosion, while the extraction of rotational energy of the newly formed black hole drives the gamma ray burst. In the latter, magnetic fields are the agent driving the process.

In this article, we study the gravitational collapse and formation of the Kerr black hole from the rotating progenitor star. We follow the evolution of black hole spin, coupled with its increasing mass. We study the effect of different level of rotation endowed in the progenitor's envelope, and we put some constraints on the final black hole parameters.

Our method is based on semi-analytical computations that involve stellar-evolution models of different progenitors. We also follow numerically the black hole evolution and spacetime metric changes during the collapse, via General Relativistic MHD modeling.

**Keywords:** Black hole physics – magnetic fields – accretion

## 1 INTRODUCTION

Stellar mass black holes reside in transient and persistent X-ray sources. Transient X-ray sources transform the gravitational potential energy of the black hole into radiation of

the accretion disk, fed by the companion star. From the analysis of the orbital motion in the binary, astronomers obtain information about the gravitational mass, and an estimate of the mass of the black hole. The typical masses of these black holes are around 6-10 Solar mass, while the most massive electromagnetic black holes have masses of  $20 M_{\odot}$  (Reynolds, 2019). Various methods of spin estimates utilize the spectral analysis of radiation from the accretion disk, namely the continuum fitting method or the X-ray reflection spectrum modeling. These methods give consistent results but with a wide range of spin determinations for individual black holes, from  $a = 0.3$  to  $a \gtrsim 0.95$ .

The newly born black holes are engines of gamma ray bursts. These very energetic events have a transient nature and are associated with a catastrophic collapse of the star. The accretion power is transformed to the bulk kinetic energy of the jet launched along the rotation axis of the black hole. This black hole must be at least moderately or very highly spinning  $a \gtrsim 0.6 - 0.9$  in order to provide an efficient power generation for the jet.

Apart from electromagnetic observations, black holes in the Universe are detected via gravitational wave window. The existence of gravitational waves is predicted by General Relativity. The accelerating objects generate changes in the spacetime curvature which propagate outwards with the speed of light. These propagating ripples are called waves, and the observer on Earth will also find the spacetime distorted once such a wave reaches the Solar System. In the gravitational wave detectors, the strain is a measured displacement between the test masses, relative to the reference length. The analysis of the signal is done via numerical relativity methods, and it enables determination of the masses and projected spins of compact objects whose coalescence is being observed.

Since 2015, the binary compact object mergers, including stellar mass black holes, have been detected many times. These discoveries brought new information about the masses and estimated spins of the black holes produced from stellar progenitors. In LIGO data, a negative correlation between the black hole masses and the mean effective spins is found (Safarzadeh et al., 2020). In general, the LIGO measurements disfavour large spins. Typical spins are constrained to  $a \lesssim 0.4$ . For aligned spins, these constraints are tighter, and results suggest  $a \sim 0.1$ . On the other hand, masses of black holes detected through gravitational waves are systematically larger than previously known. Most of them seem to be around  $20 - 30 M_{\odot}$ , while the most massive event detected recently was fitted with two black holes weighing about 66 and 85 Solar masses (GW 190521).

In this contribution we are interested in quantifying the gravitational collapse of a massive star and determination of the mass and spin of the newly formed black hole. Our analysis shows that these two quantities are anti-correlated and depend on the angular momentum content in the collapsing envelope.

We build our study following a series of works that have been previously published (Janiuk and Proga, 2008; Janiuk et al., 2008, 2018; Murguia-Berthier et al., 2020). In particular, Janiuk and Proga (2008) and Janiuk et al. (2008) explored the problem of how fast the black hole can spin up via the collapse. This study addressed the long GRB as a luminous transient powered by the spinning black hole. Depending on the accretion scenario and the angular momentum content in the envelope, the maximum duration of the GRB event can be determined. Basic condition that has to be satisfied for a successful GRB, is that some part of the rotating envelope must contain enough angular momentum

to exceed the critical limit:

$$l_{\text{spec}} = l_0 f(\theta) g(r) \quad (1)$$

where the normalization is scaled to  $l_0/l_{\text{crit}} = x$ .

$$l_{\text{crit}} = \frac{2GM}{c} \sqrt{2 - a + 2\sqrt{1 - A}} \quad (2)$$

where  $A$  is the black hole dimensionless spin parameter. The rotating torus and BH spin drive the GRB central engine, as long as the torus angular momentum is above the critical value (Janiuk et al., 2008).

Various authors (Lee and Ramirez-Ruiz, 2006; Barkov and Komissarov, 2010) studied the properties of rotating collapsar envelope in the context of long gamma ray bursts. In particular, also spin-up of the envelope by a companion can be a source of enhanced rotation to prolong the duration and/or provide more power to the transient. Some results suggest that the binary companion black hole merged with the collapsar's core might lead to a gravitational wave event accompanied by a bright gamma ray burst (Janiuk et al., 2017). On the contrary, other studies show that a certain fraction of massive O-type stars can vanish without a trace (i.e. without a bright luminous transient), if only the slow rotation of those stars prevents them from gaining an effective feedback from accretion disk (Murguía-Berthier et al., 2020).

## 2 THE MODEL SET-UP

To describe the process of collapse in a proper way, we would need to start from the matter distribution of an evolved star, and then follow gravitational collapse by solving the Einstein equations for matter-field evolution, until the massive Kerr black hole is finally formed and all matter is either accreted or expelled because of energy deposition, possible due to the shock waves or magnetic reconnections. Such computations are currently beyond the scope of theoretical and numerical astrophysics.

Some efforts have been made already to simulate a collapsar and involve the conservation equation for the stress–energy tensor. They include the fluid and radiation fields, and the metric evolution followed through the standard BSSN method. However, the black hole growth was not followed in these works and the simulations stopped after the core collapse (Ott et al., 2018). If the black hole was found and diagnosed by means of the baryon mass enclosed inside a certain radius, this radius was identified with the Schwarzschild radius, i.e. the black hole was by definition a non-rotating one. Its mass is then fixed and also the metric is frozen (Kuroda et al., 2018).

In our approach, we focus on the further evolution of the black hole parameters, namely its spin and mass, which are affecting also the Kerr metric changes. Our approach is therefore more precise than in the above cited works, as for the dynamical evolution studied in General Relativity. On the other hand, the cost of this approach is a big simplification of the matter field distribution. We are trying to tackle this problem in two ways.

## 2.1 Matter configuration

First, we adopt the density distribution that is resulting from physical model of the pre-supernova star, pre-calculated by means of the stellar evolution model. Second, we adopt a spherical density distribution resulting from the radial accretion problem (i.e. the Bondi solution). In both cases, we supply the collapsing cloud with a small angular momentum, concentrated on the equatorial plane, so that the star is rotating. Furthermore, in the Bondi case, we equip the star with magnetic fields of a chosen geometry and strength. We study the gravitational collapse as the sequence of quasi-stationary Kerr solutions for a growing mass and changing spin of the black hole. The spin is changing because of rotating matter is adding the angular momentum after it is transmitted through the black hole horizon.

Computations of the self-similar solutions based on the pre-computed stellar evolution tables are performed with the numerical code adopted from (Janiuk and Proga, 2008). The magnetized Bondi case is studied by means of the full general relativistic magneto-hydrodynamical simulation, i.e. here the stress-energy tensor contains both matter and electromagnetic parts. Numerics is tackled here with the generic MHD algorithm adopted from the HARM code (Gammie et al., 2003) and further developed by (Janiuk et al., 2018). This code is working in the MPI-parallelized version on the supercomputing clusters and the evolutionary scheme is supplemented with the Kerr metric update embedded in the code, as developed in 2018 by our Warsaw group.

### 2.1.1 Density distribution in a pre-supernova star

We use the pre-supernova models from Woosley and Weaver (1995) and also newer ones from Heger et al. (2000); Woosley et al. (2002) and Heger et al. (2005). The ZAMS mass of the star is  $25 M_{\odot}$ . First two of them did not take into account rotation during the stellar evolution modeling, and neglected magnetic fields. The initial metallicity was  $10^{-4}$ , so the mass loss was negligible. The third star model is magnetized.

The density distribution in these pre-supernova models is shown in Fig. 1. Subsequent layers of elements synthesized in the stellar interior are traced by this density profile. The innermost layer, consisting of pure Iron, is forming the core that represents initial black hole born just at the start of collapse. The mass of this core is equal to  $1.4 M_{\odot}$ . The thin Silicon shell located outside this layer accretes first. Further heavy shells are then made of Oxygen with some contribution of Neon, Magnesium and Carbon, and accrete on the newly born black hole. The outermost Helium shell accretes at the core at later times. The Hydrogen envelope, located above radius of  $r \gtrsim 10^{11}$  cm, can be either accreted or expelled.

### 2.1.2 Spherically symmetric inflow

We assume initially that the angular momentum of accreted fluid is negligible and its velocity has a non-vanishing component only in the radial direction. The equation of continuity gives  $4\pi r^2 \rho(r) u^r(r) = -\dot{M}$ , where the constant on the right-hand side has a meaning of mass accretion rate.

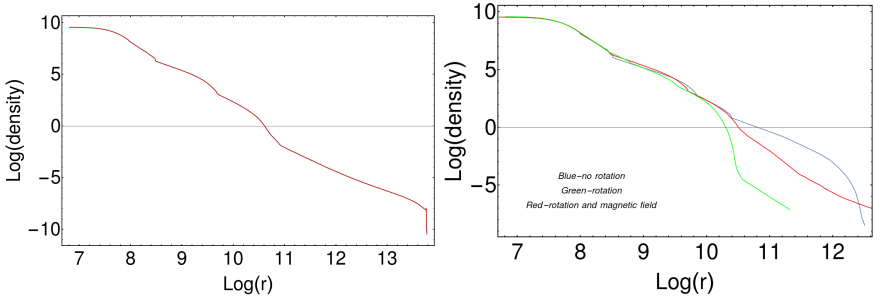


**Figure 1.** Density distribution in the pre-supernova stars used in our modeling. **Left:** Pre-SN spherically symmetric stellar model from [Woosley and Weaver \(1995\)](#) taken as initial condition for homologous collapse simulation of [Janiuk and Proga \(2008\)](#). **Right:** three other pre-SN stellar models, taken from [Heger et al. \(2000\)](#); [Woosley et al. \(2002\)](#), and [Heger et al. \(2005\)](#). These latest models include rotation or magnetic fields in the stellar evolution calculations.

The distribution of density as the function of radius comes from the solution of transonic accretion flow in spherical geometry. The initial density profile and the radial component of the velocity ( $u^r$ ) of the material is determined by the relativistic version of the Bernoulli equation ([Hawley et al., 1984](#)). In this formalism, the critical point ( $r_s$ ), where the flow becomes supersonic, is set as a parameter. Here we take the value of  $r_s = 80r_g$ . The fluid is considered a polytrope with a pressure  $P = K\rho^\gamma$ , where  $\rho$  is the density,  $\gamma = 4/3$  is the adiabatic index, and  $K$  is the constant specific entropy. Once the critical point,  $r_s$ , is set, the velocity at that point is:

$$(u_s^r)^2 = \frac{GM}{2r_s}, \quad (3)$$

where  $r$  is the radial coordinate,  $M$  is the mass of the BH and the sound speed is:

$$c_s^2 = \frac{\gamma \frac{P_s}{\rho_s}}{1 + \frac{\gamma}{\gamma-1} \frac{P_s}{\rho_s}}. \quad (4)$$

The constant specific entropy can be obtained using the sound speed:

$$K = \frac{c_s^2}{\rho^{\gamma-1}\gamma} \quad (5)$$

The radial velocity profile is obtained by numerically solving the equation ([Shapiro and Teukolsky, 1986](#)):

$$\left(1 + \frac{\gamma}{\gamma-1} \frac{P}{\rho}\right)^2 \left(1 - \frac{2GM}{r} + (u^r)^2\right) = \text{constant} \quad (6)$$

The radial velocity is given by:

$$(u^r)^2 = \frac{GM}{2r}. \quad (7)$$

Finally, the accreting material is endowed with small angular momentum scaled to the one at the circularisation radius of  $r_{\text{circ}}$ , being the ISCO radius (equal to  $6 r_g$  for a non-rotating black hole; see (Janiuk et al., 2018)). It is also scaled with polar angle to have its maximum value on the equatorial plane, at  $\theta = \pi/2$ :

$$l = S l_{\text{isco}} r^2 \sin^2 \theta \quad (8)$$

where  $l$  is the specific angular momentum, defined as  $l = u^\phi r^2$ ,  $l_{\text{isco}}$  is the specific angular momentum at the ISCO of the black hole, and  $\theta$  is the polar coordinate.

### 3 STRONG GRAVITATIONAL FIELDS

Gravitational field of a black hole is described by Kerr metric, which can be written in the well-known Boyer-Lindquist coordinate system  $(t, r, \theta, \phi)$  and the metric element is given by:

$$\begin{aligned} ds^2 = & - \left( 1 - \frac{2Mr}{R^2} \right) dt^2 - \frac{4Mra \sin^2 \theta}{R^2} dt d\phi + \\ & + \left( r^2 + a^2 + \frac{2Mra^2}{R^2} \sin^2 \theta \right) \sin^2 \theta d\phi^2 + \frac{R^2}{\Delta} dr^2 + R^2 d\theta^2 \end{aligned} \quad (9)$$

where  $R^2 = r^2 + a^2 \cos^2 \theta$ ,  $\Delta = r^2 - 2Mr + a^2$ . The inner horizon is located at  $r_{\text{H}} = 1 + (1 - a^2)^{1/2} M$ , with  $a = J/M$ , and the condition about the presence of the outer event horizon leads to the maximum value of the dimensionless spin,  $|a| \leq 1$ . Note that here the convention is used with  $G = c = 1$ . Here  $M$  denotes mass of the black hole, and the spin parameter  $a$  of the Kerr metric describes its rotation. This spacetime is asymptotically flat and the region far away from the ergosphere and event horizon experiences a negligible gravitational influence.

In Kerr metric the axial symmetry about the rotation axis is assumed and the metric elements are stationary in time. The very strong gravitational distorsion becomes infinite and forms a singularity below the event horizon.

#### 3.1 Evolution of Kerr metric

The mass and spin of the black hole are rapidly changing during the collapse process. In the numerical simulations we update therefore the six non-trivial coefficients of the Kerr metric, according to the change of these quantities. We neglect however the self-gravity of the accreting fluid, and we assure that the only source of gravitational potential is the dynamically changing black hole mass,  $M + \Delta M$ :

$$\Delta M = \frac{M^t}{M^0} - 1 \quad (10)$$

Also, the black hole spin changes according to the inflow of angular momentum from the rotating envelope. Hence,

$$\Delta a = \left( \frac{J}{M^t} - \frac{a^{t-dt}}{M^t} \dot{E} \right) \Delta t \quad (11)$$

where  $M^t$  denotes the current black hole mass at time  $t$ ,  $M^0$  denotes initial black hole mass, and  $\dot{J}$  and  $\dot{E}$  are the flux of angular momentum and energy flux transmitted through the black hole horizon at a given time (Janiuk et al., 2018). The six non-trivial components of the Kerr metric, namely  $g_{tt}$ ,  $g_{t\phi}$ ,  $g_{t\phi}$ ,  $g_{r\phi}$ ,  $g_{\phi\phi}$ , are updated at every time step and they get new values. This is a simplified treatment of the process, and new simulations with the self-gravity effects taken into account are planned to be the subject of our future work (Palit et al., in prep.).

## 4 MAGNETIC FIELDS

In order to initiate the numerical code we employ an initially parabolic magnetic field which is fully described by the only non-vanishing components of the four-potential,

$$A_\phi \propto (1 - \cos(\theta)) \quad (12)$$

in dimension-less Boyer-Lindquist coordinates. The magnetic field (and the associated electric component) are generated by currents flowing in the accreted medium far from the black hole, as the latter does not support its own magnetic field. The four-potential vector components define the structure of the electromagnetic tensor,  $F_{\mu\nu} \equiv A_{[\mu,\nu]}$ ; by projecting onto a local observer frame one then obtains the electric and magnetic vectors  $\mathbf{E}$  and  $\mathbf{B}$ . From the simple initial configuration, the numerical solution rapidly evolves into a complex entangled structure, with field lines turbulent within the accreting medium. At the end of the simulation, while the matter gets accreted into black hole and almost empty envelope remains, the field lines become more organized again.

## 5 RESULTS

### 5.1 Homologous mass accretion in collapsar

The original paper by Janiuk and Proga (2008) included four models of the angular momentum profile, but did not consider the black hole spin changes during the collapse. Then the subsequent work Janiuk et al. (2008) examined the black hole spin evolution, with the number of models of angular momentum distribution limited to two cases. Here we present the results of calculations for one of the models which was not included in the second paper, with the angular momentum profile described by the function:

$$f(\theta) \propto \sin^2(\theta). \quad (13)$$

with several normalizations with respect to the critical value,  $l_{crit}$  (see (2)):  $x = 0.4$ ,  $x = 1.0$  and  $x = 1.4$ . Note that the same values are used in GRMHD simulations presented in next Section.

In this particular model we allowed for accretion of matter with super- and sub-critical angular momentum at the same time, thus referring to a homologous accretion scenario. We also did not terminate our calculations after there was no matter with sufficient amount of

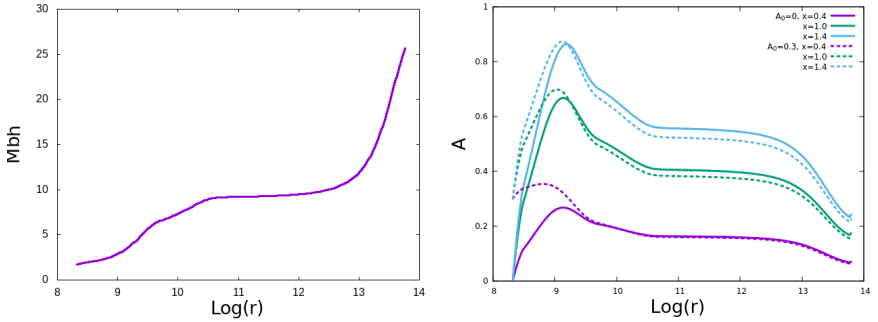


**Figure 2.** BH mass (left) and spin evolution (right) during collapse. Initial density distribution is taken from the  $25 M_{\odot}$  pre-supernova model of [Woosley and Weaver \(1995\)](#). Accretion scenario assumes homologous collapse with black hole spin-up, starting from either spin-less or moderately spinning core ( $A_0 = 0$  or  $A_0 = 0.3$ ). Initial core mass is  $1.4M_{\odot}$ . Angular momentum in the envelope is maximum at the equator, and scales with polar angle as  $\sin^2 \theta$ , where  $\theta = 0$  and  $\theta = \pi$  refer to the poles. Normalisation of rotation with respect to the critical value, see (2), is denoted with  $x = 0.4, 1.0$  and  $1.4$  (see blue, green and cyan lines in the right panel).

angular momentum to sustain the torus, so that no part of the Hydrogen envelope was expelled, and finally all the mass is accreted. We performed the calculations for two values of the initial black hole spin:  $A_0 = 0$  and  $A_0 = 0.3$ . The spin and the black hole mass evolution are shown in Fig. 2. The black hole mass increase is the same for all the  $x$  normalization values, because matter with sub- and super critical angular momentum accrete together. The black hole spin evolution depends on both initial spin and initial angular momentum of the matter. In case of  $x = 0.4$  maximal spin is significantly higher for  $A_0 = 0.3$  than for a non-spinning black hole. The difference between maximal spin values in the models with  $A_0 = 0.3$  and  $A_0 = 0$  is smaller for higher  $x$ . In general, we note that the spin starts to increase immediately at the beginning of the calculations, and the lower  $x$  value is, the faster the spin reaches its maximum and then starts to decrease. The final spin value does not depend on the  $A_0$ .

## 5.2 MHD evolution of slowly-rotating inflow with Kerr metric update

In the *HARM* code GR MHD simulations, we set the outer boundary of the computational domain at the radius  $10^3 r_g$ , where the inflow is purely radial at initial time. The inner boundary is set at  $\approx 0.98 r_H$ , i.e. at below the horizon radius for the corresponding value of spin  $a$ . The grid domain has been resolved at  $256 \times 256$  points in  $(r, \theta)$  coordinates. In MHD models, we renormalize the magnetic intensity to determine the plasma parameter  $\beta = p_{\text{gas}}/p_{\text{mag}}$  (smaller  $\beta$  corresponds to a more magnetized plasma).

Because of the perfect conductivity and the force-free approximation (apart from the effective small-scale numerical dissipation), the magnetic field lines remain attached to plasma. During the evolution, the  $\beta$ -parameter is not uniform across the computational domain and it changes in time. In the limit of negligible magnetization ( $\beta = \infty$ ) the grav-

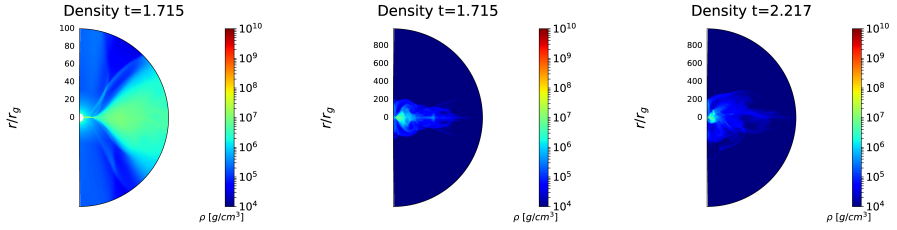


**Figure 3.** Density distribution in the late time of the simulation. Model parameters: black hole initial spin  $A_0 = 0.5$ , critical rotation parameter,  $S = 1.0$ . Model neglects magnetic fields. Rotationally supported disk-like structure is present for a long time in the equatorial plane. Note the different spatial scale of the left panel, which shows a zoom-in of the middle figure.

itational attraction of the black hole prevails. But in the case of equipartition between the magnetic and hydrodynamic pressure ( $\beta \approx 1$ ) near the horizon the accretion rate is diminished (cf. Karas et al. (2020), *this Proceeding*).

Our collapsar simulations start from a spherically symmetric distribution of density of a purely radial infall, which is quickly broken by the imposed rotation. The flow concentrates towards the equator, forming a mini-disk structure. The flow is supersonic near the black hole horizon, and in many cases, the multiple sonic surfaces are found with an aspherical shape (resembling an *eight-letter*). This feature refers to the inner sonic surface which after some time gets accreted. In the models with critical and supercritical rotation ( $S \gtrsim 1.0$ ), this initial transient shock is accompanied with some moderate variability of the accretion rate. Another sonic surface, located initially at  $80 r_g$ , expands outwards. The expanding shock velocity is typically much lower than the escape velocity at the shock radius.

The densest part of a rotationally-supported mini-disk is enclosed within a small region of  $r < 20r_g$  (cf. Murguía-Berthier et al. (2020)). The sub-critical models ( $S \leq 1.0$ ) do not contain enough angular momentum to form a mini-disk bubble, and the material from both polar regions and equator can contribute to accretion and black hole mass grows more quickly in these models. In case of super-critical accretion, only material from polar regions accretes, while the angular momentum cannot be transported if magnetic fields are neglected. The accretion rate in this case is rather low for the first part of the simulation, while it grows later, when the bulk of material falling from the outer parts of the envelope reaches the mini-disk and is able to overpass it above and below the equatorial plane. This phase (reached typically after  $t > 0.8 - 1$  s, in physical time units) is also associated with large spikes in the accretion rate. The mini-disk is destroyed, nevertheless in many simulations we observe the existence of a long-living disk-like structure in the equatorial plane, which is sustained until the end of the simulations (typically  $t_{end} = 2$  s). The detailed shape, and time for which the feature is preserved, depends also somewhat on the value of initial black hole spin  $A_0$  (for the highest probed value,  $A_0 = 0.85$ , we found the longest timescale of disk structure,  $t_f = 4.5$  s; see (Król and Janiuk, 2020)). In Fig. 3 we show the density distribution in the late phase of the simulation, for one exemplary model. Parameters of this model are  $A_0 = 0.5$  and  $S = 1.0$ .

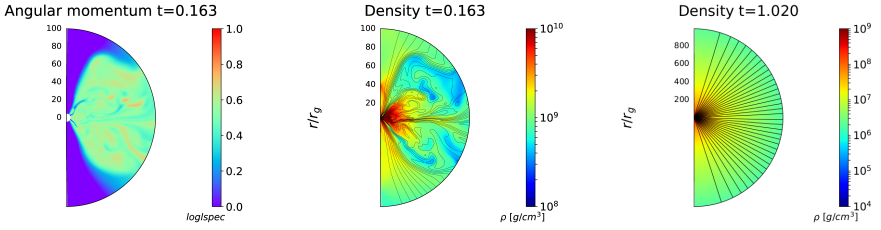


**Figure 4.** Results for magnetized model, with  $\beta = 1$ , initial black hole spin  $A_0 = 0.5$  and critical rotation parameter,  $S = 1.0$ . Figures show angular momentum distribution and density field with overplotted magnetic field lines at the beginning of the simulation (left and middle panels) and the density structure, at the end of the simulation. Note the different spatial scale of the right panel, which shows a zoom-out of the middle figure.

The evolution of the black hole spin is non-linear, as the rotation of the black hole can both speed up and slow down, depending on the amount of angular momentum that is reaching the horizon. The maximum value of the spin reached during the collapse temporarily, as well as the final value, depends also on the assumed initial spin. For sub-critical rotation models, only for smallest value of  $A_0 = 0.3$  we observed a temporal spin-up of the black hole (up to  $A \sim 0.4$ ), while the end value was below the starting one ( $A_f \sim 0.15$ ). For super-critical rotation, the black hole could even spin-up maximally for some period of time, but finally the spin was smaller. Typically  $A \sim 0.7$  was reached in case of angular momentum in the envelope normalised to  $S = 1.4$ , which means that effectively the highly spinning black hole at  $A_0 = 0.85$  did spin-down after the collapse.

The final black hole masses are obviously limited by the total mass of the envelope, assumed always to be  $25 M_\odot$ . They were between  $M_{BH}^{end} = 11$  and  $18 M_\odot$  at the end of the simulation, and in non-magnetized models the largest black hole masses were obtained for sub-critical rotations, which also correlates with the smallest final spins. These values did not differ much between the models with various initial spins. For super-critical rotation of the envelope, the final black hole mass was smaller, and also decreased for large initial black hole spins.

In order to reveal the changes of the magnetic field near the black hole, we study the evolution of the strongly magnetized plasma, that is inflowing into the horizon. In Fig. 4 we present the MHD simulation results. Parameters of rotation in the envelope and initial black hole spin are the same as in Fig. 3, but now the model is magnetized, and the magnetic to gas pressure ratio in the accreting cloud is equal to  $\beta = 1$ .

As mentioned above, the initial configuration is the parabolic magnetic field solution, but this configuration starts quickly changing once the inflowing plasma arrives in the domain, while the magnetic field is coupled to matter. The purely poloidal field changes and develops a strong toroidal component (see Fig. 5).

We observe also that the magnetized jet wants to form in the polar regions, where the open field lines are visible in the early stage of evolved configuration, together with dense and turbulent torus structure in the equatorial plane (time  $t \sim 0.1 - 0.15$  s). Nevertheless, because of large density in the envelope, the jet cannot break out of the collapsing star.

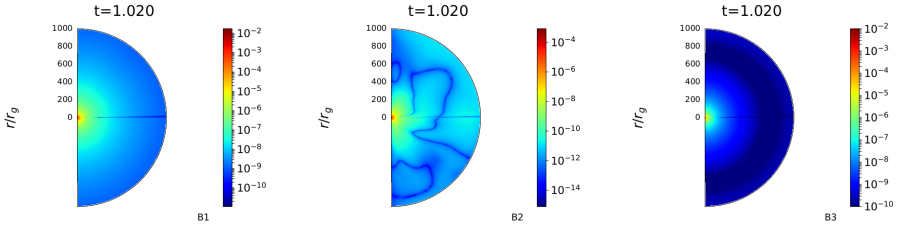


**Figure 5.** Components of magnetic field 3-vector, at the late stage of the simulation. Parameters of the run:  $\beta = 1$ , initial black hole spin  $A_0 = 0.5$ , envelope rotation  $S = 1.0$

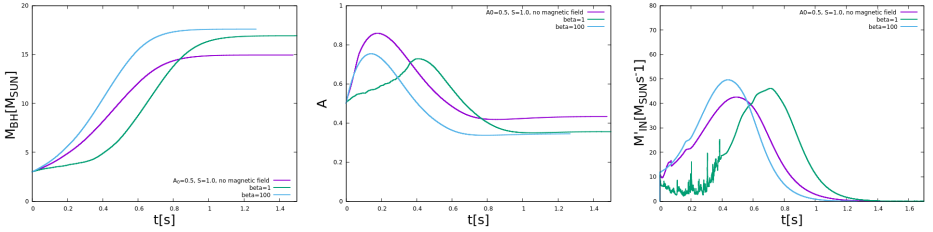


**Figure 6.** Evolution of the black hole mass, its spin, and accretion rate onto BH horizon, during the simulation. Parameters of the run: initial black hole spin  $A_0 = 0.5$ , envelope rotation parameter  $S = 1.0$ . Non-magnetized models are shown with purple lines. Magnetic field in magnetized model was parameterized with  $\beta = 1$  (green lines) or  $\beta = 100$  (cyan lines).

The polar funnels are baryon-polluted, and quickly change the magnetic field configuration back to radially-dominated, and the equatorial configuration of matter turns back to quasi-spherical (at time  $t \sim 0.5$  s). We envisage, that full 3-dimensional simulations might be needed to overcome this problem and allow to sustain a long-living, dense and magnetized torus together with a jet-like funnel.

We also probed the effects of magnetic fields on the accretion rate, black hole spin, and mass in the collapsar models. In Fig. 6 we show the evolution of these quantities, for initial spin  $A_0 = 0.5$  and the critical rotation parameter  $S = 1.0$ . Parabolic magnetic field was normalized to  $\beta = 1$  or  $\beta = 100$ . For comparison, non-magnetized model of the same parameters but  $\beta = \infty$  is presented in the Figure. The main quantitative difference is that the black hole spin is always smaller at its maximum in the magnetized models, than in the non-magnetized, for the same set of other parameters. The final black hole spin is also smaller if magnetic fields are included. On the other hand, the mass of the black hole achieved larger values. This is the result of angular momentum transport via magnetic fields, which allows matter to accrete not only from the polar regions, but also through the rotating disk. The variability of accretion rate is more visible in the weakly magnetized case ( $\beta = 100$ ) than in the strongly magnetized. We suggest that this is an effect of a very strong magnetic barrier in the latter.

## 6 CONCLUSIONS

- We compute the collapsar model with slowly-rotating quasi spherical collapse with changing black hole spin and mass and Kerr metric update. We probed a range of angular momentum contents in the collapsars envelope, and range of initial black hole spins.
- Our method to follow collapse is fully GR MHD, while still not by exactly solving the Einsteins equations, but it gives a good approximation to this problem
- Our test models out some constraints on the angular momentum content of the collapsing progenitor star, with the resultant mass and spin of the BH.
- For supercritical rotation, we always observe spin up of the black hole at some stage of the simulation. The dependence on the initial black hole spin is however not monotonic, and at the end of simulation, the black hole can be effectively spun down with respect to the initial spin value.
- The strongly magnetized collapsars reach lower maximum black hole spins, and even for supercritical rotation in the envelope, the black hole may not reach the maximum Kerr parameter.
- The growth of the black hole mass is largest when the envelope rotation is slow, and when the black hole was at least moderately spinning initially.
- Two shock fronts were found with velocities are  $0.014 c$  and  $0.022 c$ . For the models with sub critical envelope rotation we obtained higher velocities of the shock fronts:  $0.04 c$  and  $0.044 c$ , depending on BH spin ( $A_0 = 0.5, 0.85$ ). This trend seems opposite in comparison to [Murguia-Berthier et al. \(2020\)](#) who studied non-spinning BHs.

## ACKNOWLEDGEMENTS

The authors thank Daniel Proga for helpful discussion. AJ was supported by grant no. 2019/35/B/ST9/04000 from the Polish National Science Center, and acknowledges computational resources of the Warsaw ICM through grant Gb79-9. DK was supported by Polish NSC grant 2016/22/E/ST9/00061.

## REFERENCES

- Barkov, M. V. and Komissarov, S. S. (2010), Close binary progenitors of gamma-ray bursts, *MNRAS*, **401**(3), pp. 1644–1656, [arXiv: 0908.0695](#).
- Gammie, C. F., McKinney, J. C. and Tóth, G. (2003), HARM: A Numerical Scheme for General Relativistic Magnetohydrodynamics, *ApJ*, **589**(1), pp. 444–457, [arXiv: astro-ph/0301509](#).
- Hawley, J. F., Smarr, L. L. and Wilson, J. R. (1984), A numerical study of nonspherical black hole accretion. I Equations and test problems, *ApJ*, **277**, pp. 296–311.
- Heger, A., Langer, N. and Woosley, S. E. (2000), Presupernova Evolution of Rotating Massive Stars. I. Numerical Method and Evolution of the Internal Stellar Structure, *ApJ*, **528**(1), pp. 368–396, [arXiv: astro-ph/9904132](#).
- Heger, A., Woosley, S. E. and Spruit, H. C. (2005), Presupernova Evolution of Differentially Rotating Massive Stars Including Magnetic Fields, *ApJ*, **626**(1), pp. 350–363, [arXiv: astro-ph/0409422](#).
- Janiuk, A., Bejger, M., Charzyński, S. and Sukova, P. (2017), On the possible gamma-ray burst-gravitational wave association in GW150914, *NewA*, **51**, pp. 7–14, [arXiv: 1604.07132](#).

- Janiuk, A., Moderski, R. and Proga, D. (2008), On the Duration of Long GRBs: Effects of Black Hole Spin, *ApJ*, **687**(1), pp. 433–442, [arXiv: 0807.2251](#).
- Janiuk, A. and Proga, D. (2008), Low Angular Momentum Accretion in the Collapsar: How Long Can a Long GRB Be?, *ApJ*, **675**(1), pp. 519–527, [arXiv: 0708.2711](#).
- Janiuk, A., Sukova, P. and Palit, I. (2018), Accretion in a Dynamical Spacetime and the Spinning Up of the Black Hole in the Gamma-Ray Burst Central Engine, *ApJ*, **868**(1), 68, [arXiv: 1810.05261](#).
- Karas, V., Sapountzis, K. and Janiuk, A. (2020), Magnetically Ejected Disks: Equatorial Outflows Near Vertically Magnetized Black Hole, in *RAGTime 20-22: Workshops on Black Holes and Neutron Stars*, pp. 97–109.
- Król, D. Ł. and Janiuk, A. (2020), Accretion induced black hole spin up revised by numerical GR MHD simulations, *ApJ(submitted)*.
- Kuroda, T., Kotake, K., Takiwaki, T. and Thielemann, F.-K. (2018), A full general relativistic neutrino radiation-hydrodynamics simulation of a collapsing very massive star and the formation of a black hole, *MNRAS*, **477**(1), pp. L80–L84, [arXiv: 1801.01293](#).
- Lee, W. H. and Ramirez-Ruiz, E. (2006), Accretion Modes in Collapsars: Prospects for Gamma-Ray Burst Production, *ApJ*, **641**(2), pp. 961–971, [arXiv: astro-ph/0509307](#).
- Murguia-Berthier, A., Batta, A., Janiuk, A., Ramirez-Ruiz, E., Mandel, I., Noble, S. C. and Everson, R. W. (2020), On the Maximum Stellar Rotation to form a Black Hole without an Accompanying Luminous Transient, *ApJL*, **901**(2), L24, [arXiv: 2005.10212](#).
- Ott, C. D., Roberts, L. F., da Silva Schneider, A., Fedrow, J. M., Haas, R. and Schnetter, E. (2018), The Progenitor Dependence of Core-collapse Supernovae from Three-dimensional Simulations with Progenitor Models of 12–40  $M_{\odot}$ , *ApJL*, **855**(1), L3, [arXiv: 1712.01304](#).
- Reynolds, C. S. (2019), Observing black holes spin, *Nature Astronomy*, **3**, pp. 41–47, [arXiv: 1903.11704](#).
- Safarzadeh, M., Farr, W. M. and Ramirez-Ruiz, E. (2020), A Trend in the Effective Spin Distribution of LIGO Binary Black Holes with Mass, *ApJ*, **894**(2), 129, [arXiv: 2001.06490](#).
- Shapiro, S. L. and Teukolsky, S. A. (1986), *Black Holes, White Dwarfs and Neutron Stars: The Physics of Compact Objects*.
- Woosley, S. E., Heger, A. and Weaver, T. A. (2002), The evolution and explosion of massive stars, *Reviews of Modern Physics*, **74**(4), pp. 1015–1071.
- Woosley, S. E. and Weaver, T. A. (1995), The Evolution and Explosion of Massive Stars. II. Explosive Hydrodynamics and Nucleosynthesis, *ApJS*, **101**, p. 181.